Comprehensive Study of Sansalvamide A Derivatives and their Structure–Activity Relationships against Drug-Resistant Colon Cancer Cell Lines

Katerina Otrubova, Gerald Lushington,† David Vander Velde,† Kathleen L. McGuire, and Shelli R. McAlpine*

Department of Medicinal Chemistry, 1251 Wescoe Hall Rd, The University of Kansas, Lawrence, Kansas, 66045-7582

Received June 21, 2007

We report an extensive structure–activity relationship (SAR) of 62 compounds active against two drug-resistant colon cancer cell lines. Our comprehensive evaluation of two generations of compounds utilizes SAR, NMR, and molecular modeling to evaluate the key 3D features of potent compounds. Of the seven most potent compounds reported here, five are second-generation, emphasizing our ability to incorporate potent features found in the first generation and utilize their structures to design potency into the second generation. These analogs share no structural homology to current colon cancer drugs, are cytotoxic at levels on par with existing drugs treating other cancers, and demonstrate selectivity for drug-resistant colon cancer cell lines over noncancerous cell lines. Thus, we have established sansalvamide A as an excellent lead for treating multiple drug-resistant colon cancers.

Introduction

Natural products often provide lead structures for new drugs. These novel structures are critical for development of original therapeutic small molecules that target new biological pathways. Sansalvamide A (San A) is one such natural product (Figure 1). San A, which was isolated from a marine fungus (*Fusarium ssp.*), exhibits antitumor activity.[1–3] To date the synthesis of 86 analogs have been reported, 75 by us[4,5] and 11 by Silverman et al.[6] The natural product is a depsipeptide and, as such, is prone to deactivation by ring opening enzymes. To avoid this, most of the 86 analogs synthesized, including all 75 of those reported by our laboratory, were synthesized as the San A peptide derivatives (Figure 1, amino acid **4**), which are from here on referred to as "San A-amide" derivatives. Cytotoxicity of San A-amide derivatives against pancreatic,[7,6,8] colon,[3,4,9,10] breast, prostate, and melanoma cancers[6] clearly indicate San A-amide's excellent potential as a new therapeutic agent for the treatment of various cancers and support further exploration of this class of compounds. All 11 of the San A-amide derivates prepared by Silverman and co-workers contain L-amino acids (L-aas),[6,8,11,12] and these demonstrate reasonable potency against one colon cancer cell line HCT-116. They attribute potency to the placement of multiple N-methyl moieties on the macrocycle. However, our extensive studies show that the SAR in HCT-116 is not due to the placement of multiple N-methyl moieties.

For the first time, we report here an extensive structure–activity relationship (SAR) of 62 compounds against two drug-resistant colon cancer cell lines (HCT-116 and HCT-15).[13] Herein we describe a comprehensive evaluation of our two generations of compounds from a global view where we outline the three-dimensional (3D) features using NMR and molecular modeling, as well as a complete discussion of all 62 derivatives structure–activity relationships. Further, these compounds are described using data from two drug-resistant cell lines to clearly demonstrate a common mode of action against this cancer. Out of the seven most potent compounds reported here, five are second-generation compounds, emphasizing our ability to incorporate potent features found in the first generation to enhance the potency of the second generation of molecules.

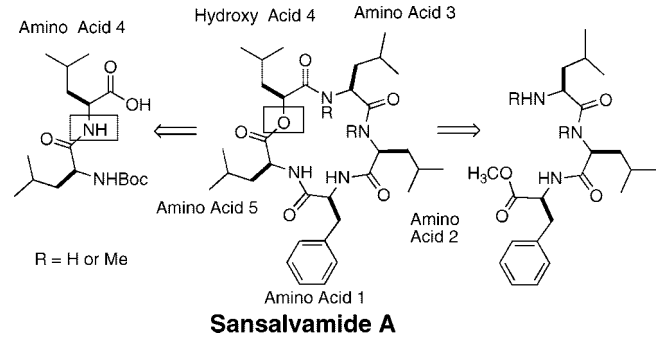

Figure 1. Retrosynthetic approach.

Our work reported below shows that there are two factors important for potency: a single N-methyl and a single D-amino acid (D-aa). This work is validated by several current examples in the recent literature where cyclic peptides and, specifically, pentapeptides with a single D-aa lock the macrocycle into a single conformation.[14,15] Further, it is well established that these cyclic pentapeptides mimic beta and gamma turns and serve as templates for appropriately positioning suitable binding motifs for proteins.[16,17] Given that we have discovered seven small molecules that target drug-resistant colon cancer cell lines at potencies that are significantly greater than those previously reported, that our derivatives share no homology with other classes of chemotherapeutic agents, that they are more potent than a current drug on the market (gemcitabine), and they have reasonable ClogP values (0.2–3.3 range)[18] and molecular weights (500–600), we feel that this class of compounds provides potential structures for further chemotherapuetic development.

Peptides are sometimes considered poor drugs for two reasons: solubility and rapid degradation within cells. For linear peptides to achieve 3D structures that will bind appropriately to their protein targets, they are often composed of extended sequences of amino acids (aas), which are insoluble. Cyclic peptides, like San A, often perform better than linear peptides

* To whom correspondence should be addressed. Shelli R. McAlpine, Department of Chemistry and Biochemistry, 5500 Campanile Road, San Diego State University, San Diego, CA 92182-1030. Tel.: 619-594-5580. Fax: 619-594-4634. E-mail: mcalpine@chemistry.sdsu.edu.

† The University of Kansas.

[a] Abbreviations: MSS, microsatellite stable; MSI, microsatellite unstable.

10.1021/jm070731a CCC: $40.75
Published on Web 01/11/2008

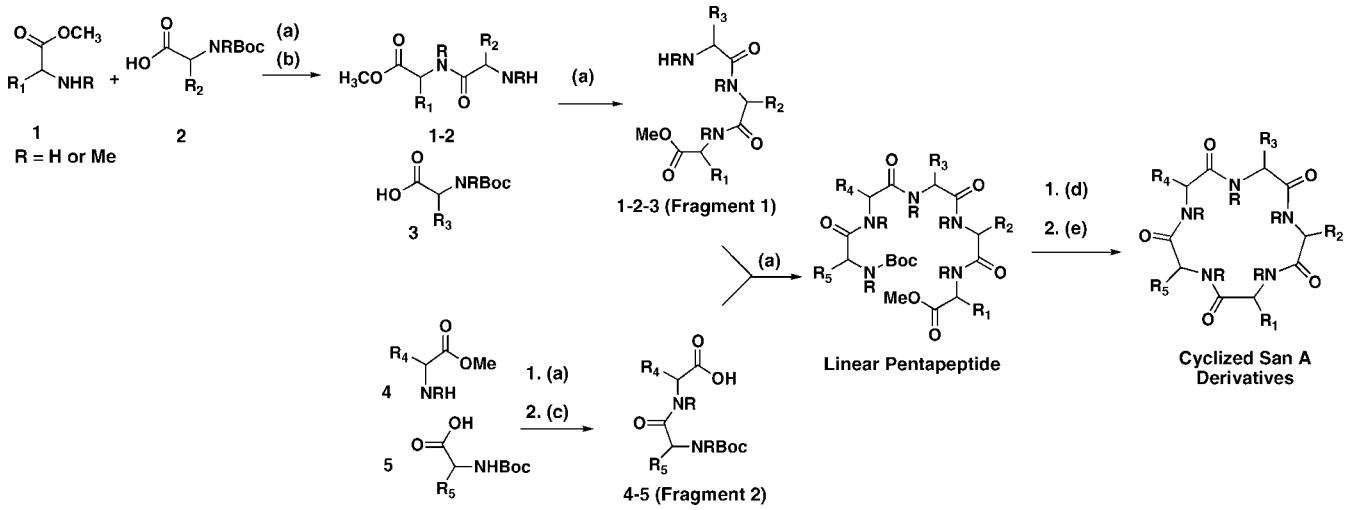

Figure 2. Synthesis of macrocycles. Conditions: (a) coupling agent,* DIPEA (3 equiv), DCM (0.1 M); (b) TFA (20%), anisole (2 equiv), DCM; (c) LiOH (4 equiv), MeOH; (d) HCl in THF (0.05 M), anisole (2 equiv); (e) HATU (0.7 equiv), DEPBT (0.7 equiv), TBTU (0.7 equiv), DIPEA (6 equiv), THF/CH_3CN/DCM (2:2:1) 0.007 M. *TBTU (1.2 equiv) and/or HATU (0.75 equiv).

because a small number of aas define a 3D structure. San A-amide analogs also have the advantage that they are lipophilic and, therefore, they have rapid membrane absorption.[19] Cyclic peptides tend to have greater binding affinity for protein targets than their linear counterparts or small molecules because they have restricted bond rotation and are conformationally constrained.[20] In addition, cyclic peptides degrade much slower than linear peptides because proteases have difficulty cleaving amide bonds located in a macrocycle.[19] In summary, cyclic peptides have commercially available chemical diversity (i.e., aas), are efficiently synthesized, have defined 3D structures that have good binding affinity for protein targets, are effective at penetrating cell membranes, and are stable within cells. To date there are 720 clinically used peptide drugs or candidates; 38% of these are in clinical trials, 56% are in advanced preclinical phases, and 5% are on the market.[21,22] These peptide drugs are used as prostate and breast cancer antitumor agents, HIV protease inhibitors, osteoporosis-treating drugs, and immunosuppressants.[23] Thus, there is outstanding precedence for treating diseases with cyclic peptides.

There is an immediate need for new drugs that provide alternatives for MSI[a] (drug-resistant) colon cancer patients. Recently, several new drugs, specifically gemcitabine, oxaliplatin, bevucizumab, cetuximab, and the tyrosine kinases inhibitors, have improved survival; however, current therapy is far from acceptable. Although major efforts have been made, few truly novel classes of compounds have been identified that have activity against drug-resistant colon cancers (MSI) tumors. This work reports our understanding of the complex structure–activity relationship of 62 San A-amide derivatives against two drug-resistant colon cancer cell lines, establishes a phenotype for cytotoxicity in cell-based assays, and connects the 3D positioning of the active compounds' side chains to growth inhibition. Further, we clearly establish that our compounds are more potent than Gemcitabine, a current drug treating these cancers.

Synthesis of San A Derivatives. The natural product, San A, is a depsipeptide, however, macrocyclic peptides possess increased stability compared to depsipeptides, and therefore, all 62 derivatives described here were constructed as the peptide analogs (Figure 1). A succinct synthetic protocol has been developed for the creation of these 62 derivatives.[4,24] These compounds provide valuable information with regards to stereochemistry, amide bond geometry, and hydrophobic, hydrophilic, and aliphatic effects on potency. Further, these derivatives have ClogP values between 0.18 and 3.3, thus meeting Lipinski's rules for solubility and effective diffusion through cellular membranes.[18] Our synthetic approach utilized a convergent solution-phase strategy to establish a reliable and inexpensive route for the large-scale production of compound needed in additional biological studies (Figure 2). As such, our outlined route provides access to the synthesis of gram quantities of these compounds.

The synthesis of the San A-amide derivatives were completed using the aas shown in Figure 3 via a synthetic strategy shown (Figure 2). We prepared two generations of compounds, wherein the first generation primarily involved the incorporation of all-L- or all-D-aa as well as N-methyl moieties at each position and the second generation included aas that involved the exchange of a single N-methyl or D-aa at each position (both generations are highlighted in Figures 4−9). The variations of each generation allowed us to explore the role of stereochemistry, amide bond geometry, and hydrophobic, hydrophilic, and aliphatic moieties. Overall, the first generation compounds allowed us to elucidate key SAR involving compounds containing all D-aas and all L-aas, while the second-generation compounds provided data on the specific role of each aa as it relates to stereochemistry, transannular hydrogen bonding, and polarity.

When 2(1*H*-benzotriazole-1-yl)-1,1,3-tetramethyl-uronium tetrafluoroborate (TBTU) and diisopropylethylamine (DIPEA) were used, acid-protected residue **1a**−**f** and *N*-Boc-protected residue **2a**−**o** were coupled to give the dipeptide 1-2-Boc (80–94% yield). Deprotection of the amine on residue **2** using TFA gave the free amine, **1** and **2** (∼quantitative yields). Coupling of the dipeptide to monomer **3a**−**n** gave the desired tripeptide (fragment 1) in good yields (80%-95%).[25] The synthesis of fragment 2 was completed by coupling residue **4a**−**g** to residue **5a**−**f** to give dipeptide **4-5-Boc**(90–95% yield). The amine was deprotected on fragment 1 using TFA and the acid was revealed in fragment 2 using lithium hydroxide. Fragment 1 and fragment 2 were coupled using multiple coupling agents,[10,26–28] yielding 75 examples of linear pentapeptides (66–90% yield).[25] In the case of the di- and tripeptide construction, acid/base workup removed excess reagents and side products, and the NMR indicated compounds did not require further purification. Only in the case of pentapeptides

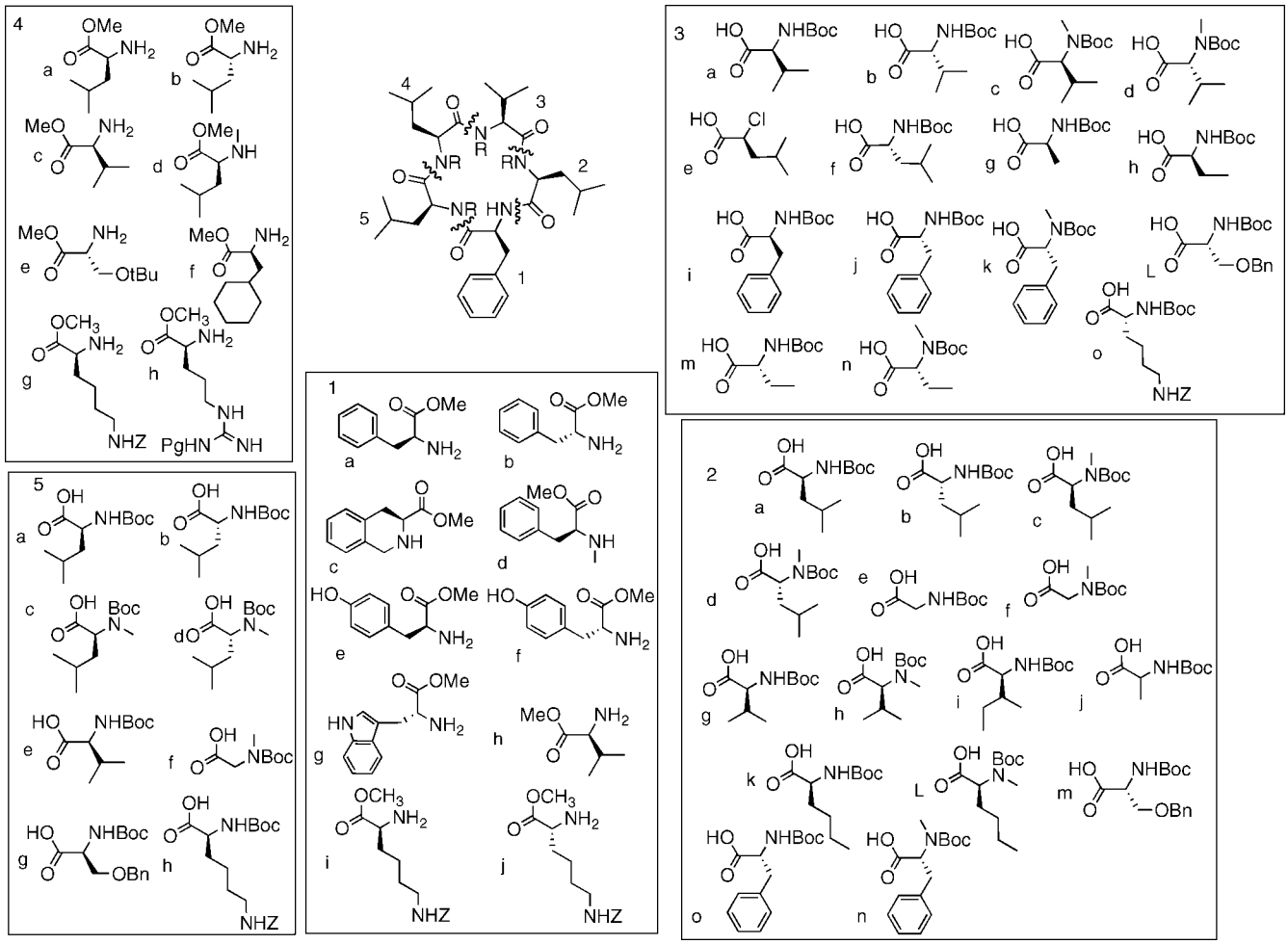

Figure 3. Amino acids used in the synthesis of 62 derivatives.

and macrocycles did we find it necessary to purify compounds via silica chromotography, making the synthesis efficient. The purity of all compounds was verified via NMR and LCMS. The linear peptides were then cyclized using conditions developed in our laboratory.[24] Upon cyclization, the final compounds were purified via flash chromatography and HPLC. When appropriate, the side chains were deprotected (serines, lysines, and tyrosines). The purity of all compounds was verified by NMR and LCMS.[24]

Structure–Activity Relationships (SAR). A total of 62 San A-amide analogs have been tested for cytotoxicity against two drug-resistant (MSI) colon carcinoma cell lines (HCT-116, HCT-15). Two cell lines were utilized to ensure that our compounds were consistently inhibiting drug-resistant colon cancers, to clearly establish structure–activity relationships (SARs), and to determine the key features necessary to inhibit growth of colon cancer cells. Potency exhibited by the San A-amide peptide (**1**) is shown so that comparisons can be made between the natural product peptide and our synthetic analogs. The histogram in Figure 4 shows the percent inhibition of growth produced by a concentration of 1 μM compound with changes at position **1** for two MSI colon cell lines. Compounds **2** and **3** are first generation compounds (shown in gray, Figure 4), while **4**−**9** are second-generation compounds (shown in black). The first generation compounds involved incorporation of a single D-aa in position **1** (**2**) or an N-methyl at **1** (**3**). It is clear from the growth inhibition that the first generation compounds with changes to position **1** are not potent (note: IC_{50}s are exponential curves therefore **2** and **3** have IC_{50}s > 50 μM in both cell lines). For the second-generation compounds in Figure 4, we incorporated a number of aas that are different from those of the natural product primarily at position **1**. Compound **4** includes an L-tetrahydroisoquinoline aa, which places a rigid aromatic moiety at **1**. Given its lack of potency, this moiety is not a positive influence on growth inhibition. Our first generation data suggested that a D-aa with an H-bonding element at **1** would potentially increase the potency, and compounds **5** and **6** were designed to determine whether a H-bond element would improve the cytotoxicity effect. Figure 4 shows that the potency of compound **5** is greatly increased compared to that of **1**, where comparison of the potency of the compounds is done using growth inhibition curves, which are exponential. The IC_{50} values of **5** and **1** (Figure 10) are 1.5 μM versus 25 μM in HCT-116 and 1 μM versus 46 μM in HCT-15, respectively. Thus, **5** is up to 50-fold more potent than **1**. Interestingly, **6** is significantly less potent than **1**, possibly due to steric interactions with the biological target. Interestingly, **7**, which contains a D-tyrosine like **5** but is also a polar element at position **4** (a lysine), has greatly reduced potency. Compound **8** involved a significant alteration in the structure, including a D-phenyl alanine at **1**, an N-methyl at **4**, and a D-leucine generated a potent compound. Comparison of IC_{50} values indicates that **8** is up to 70-fold more potent than natural product peptide **1** and up to 100-fold more potent than first generation compound **3** (Figure 10). Interestingly, compound **9**, which contains D-aas at **1**, **3**, and **4**, has limited growth inhibition against HCT-116 and no growth inhibition effect against HCT-15. Thus, overall, two compounds in the second-generation series demonstrated a clear and significant improvement in growth inhibition, **5** and **8**, where

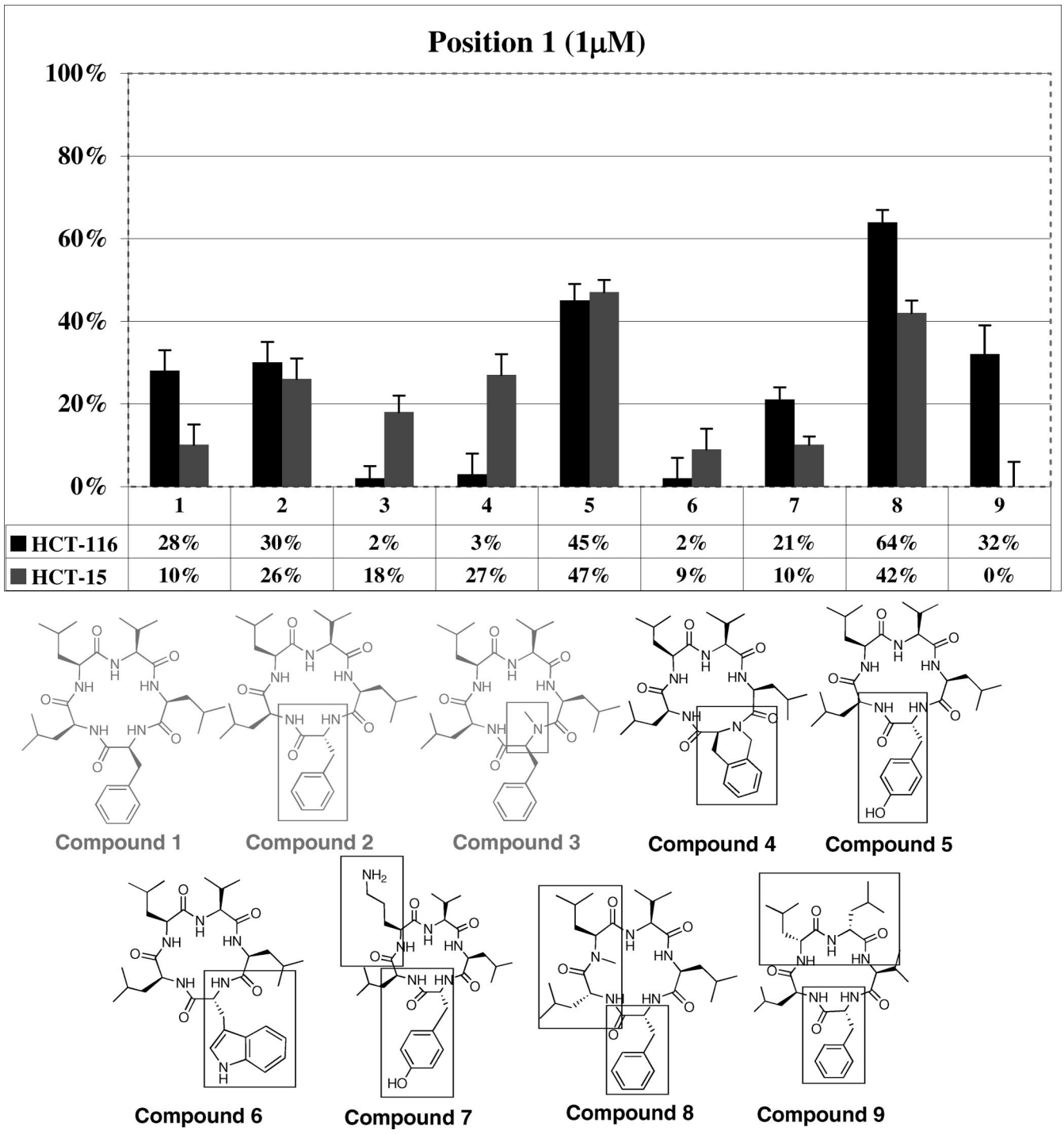

Figure 4. Compounds with changes to position **1**. Grey compounds **2** and **3** are first generation compounds, while black compounds **4**−**9** are second-generation. Each data point is an average of three wells run in three assays. Error = ±5%.

both show greater than 45% improvement against both cell lines. These two compounds showed up to 70-fold improved potency over that seen with the natural product peptide **1** and up to 100-fold improved potency over first generation compounds.

The histogram in Figure 5 shows the percent inhibition of growth by compounds with changes in position **2**. Compounds **10**−**12** are first generation compounds (shown in gray, Figure 5), while **13**−**21** are second-generation compounds (shown in black). The first generation compounds involved incorporation of an N-methyl in position **2** (**10**), a D-aa (**11**), or both (**12**). It is clear from the growth inhibition that the first generation compounds in this series do not have improved potency over the parent peptide (**1**) (note: **10**, **11**, and **12** have IC_{50}s > 50 μM in both cell lines). For the second-generation compounds, compound **13** incorporates a D-phenyl alanine at position **2** and is not potent, yet **14** contains an N-methyl D-phenyl alanine at **2** and shows nanomolar IC_{50} values (Figure 10). Both compounds **15** and **16** feature the polar residue D-serine in position **2**, where **16** also contains valine resides in positions **4** and **5** (versus leucine residues at these positions in both **15** and **1**). Both compounds are inactive compared to **14**, that is, they have IC_{50}s in the high micromolar range. Further, a more hydrophobic moiety at position **2**, for example, a benzyl oxy group that is seen in **17**, also demonstrated low potency. Additional compounds were then synthesized to investigate the impact of multiple changes to

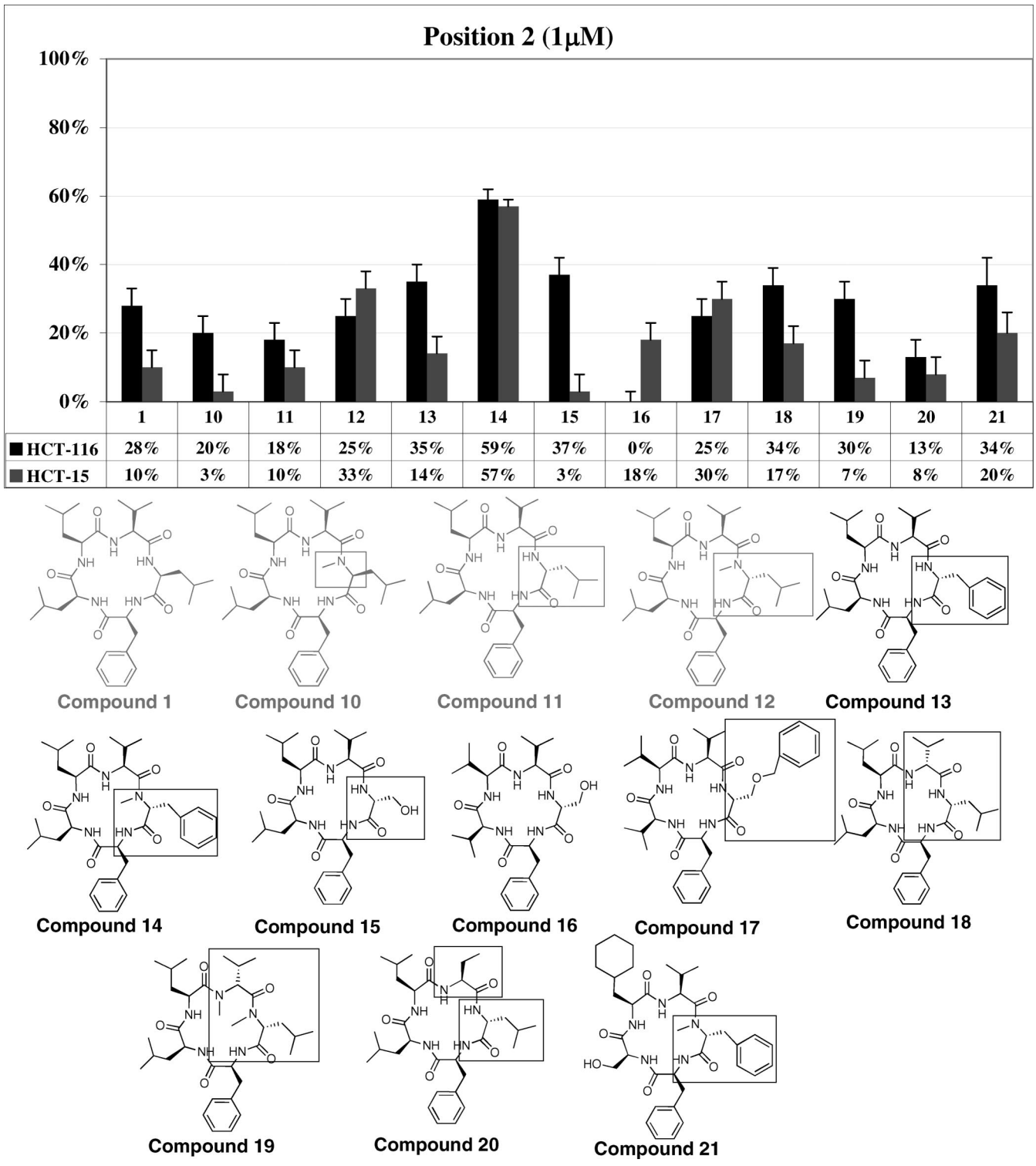

Figure 5. Compounds with changes to position **2**. Grey compounds **10**−**12** are first generation compounds, while black compounds **13**−**21** are second-generation.

the macrocyclic backbone. This included a compound with two D-aas in positions **2** and **3** (**18**) and one with N-methyl D-aas in positions **2** and **3** (**19**). Both compounds were not potent. Compound **20**, which contains a D-aa at **2** and an L-ethyl moiety at **3**, was also not potent. Finally, compound **21**, which contains an N-methyl D-phenyl alanine and is similar to **14**, but also contains a cyclohexyl moiety at **4**, similar to potent compound **45** (comprehensively discussed in Figure 7), did not have significant potency. Thus, combined features from two potent compounds (e.g., **14** and **45**) do not generate synergistic cytotoxic effects. Overall, one compound in the second-generation series demonstrated a clear and significant improvement in growth inhibition (**14**), which maintains greater than 45% against both cell lines. Comparison of the IC_{50} values of **14** and **1** (Figure 10), are 0.8 μM versus 25 μM in HCT-116 and 0.7 μM versus 46 μM in HCT-15, respectively, thus, **14** is up to 70-fold more potent than **1** and up to 100-fold more potent than first generation compound **12**, which contains an N-methyl D-leucine.

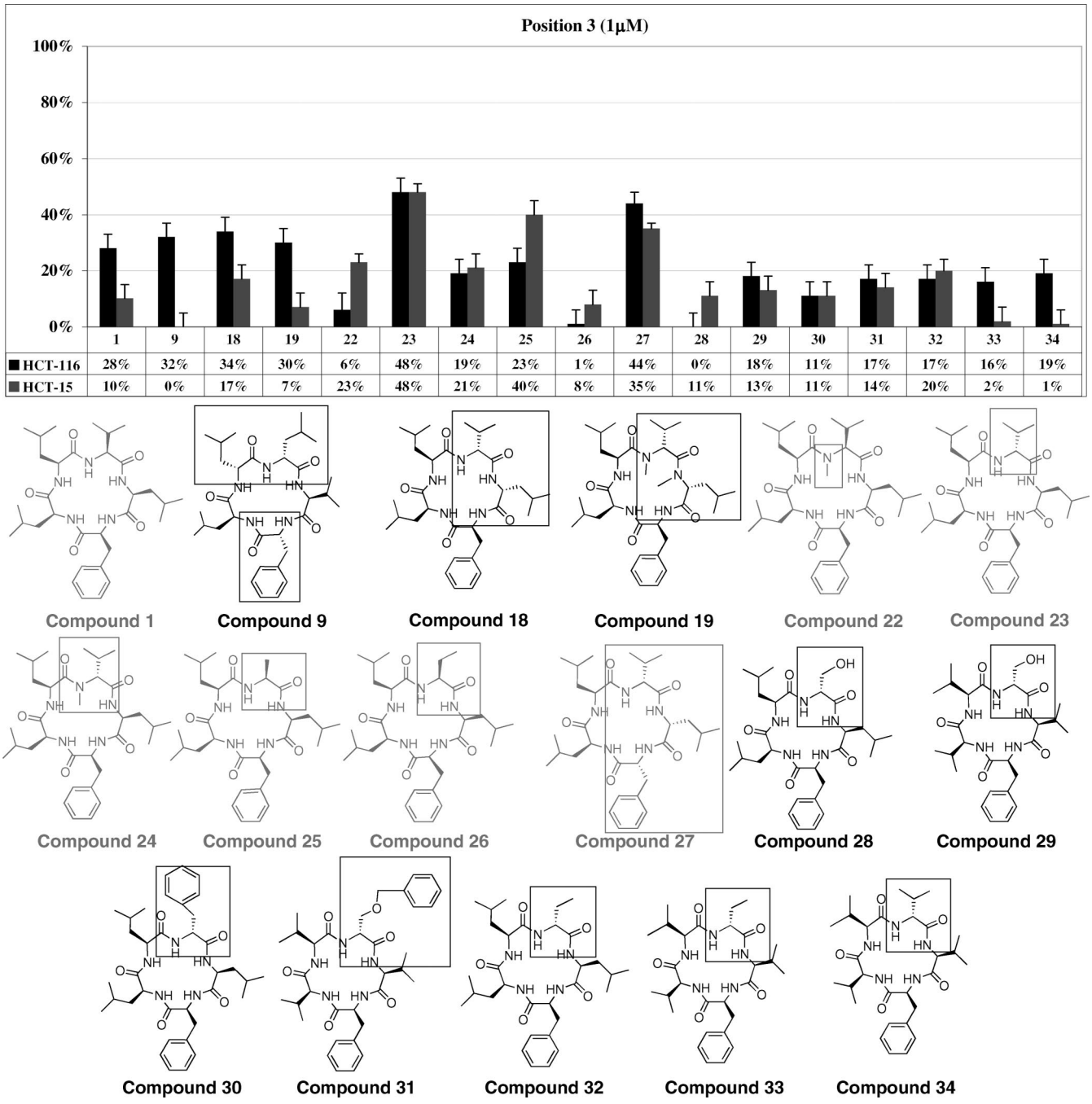

	1	9	18	19	22	23	24	25	26	27	28	29	30	31	32	33	34
HCT-116	28%	32%	34%	30%	6%	48%	19%	23%	1%	44%	0%	18%	11%	17%	17%	16%	19%
HCT-15	10%	0%	17%	7%	23%	48%	21%	40%	8%	35%	11%	13%	11%	14%	20%	2%	1%

Figure 6. Compounds with changes to position **3**. Grey compounds **22**−**27** are first generation compounds, while black compounds **9**, **18**, **19**, **28**−**34** are second-generation.

Compounds **22**−**27** are first generation compounds (shown in gray, Figure 6), while compounds **9**, **18**, **19**, and **28**−**34** are second-generation (shown in black). The first generation compounds involved incorporation of an N-methyl in position **3** (**22**), a D-aa (**23**), or both (**24**). Of these three compounds, **23** was the most active. Indeed, it shows an IC_{50} in the nanomolar range (Figure 10). In contrast to **1**, which contains an isopropyl moiety at **3**, compounds containing a methyl (**25**) or an ethyl (**26**) moiety at position **3**, were synthesized and tested. Both of these compounds showed potency of less than 45% inhibition at 1 μM against our cell lines. For the second-generation compounds, **25**, **26**, and **20** involved alterations at both position **2** and **3** and their potency is discussed earlier. Both compounds **28** and **29** feature the polar residue D-serine in position **3**, where **29** also contains valine resides in positions **4** and **5** (versus leucine residues at these positions in both **28** and **1**). Both compounds are inactive and have IC_{50}s in the high micromolar range. Compound **30** is similar to potent compound **23**, which has a D-leucine at **3**, but rather it contains a D-phenylalanine at **3**. In parallel, the cytotoxicity of **31** was tested, where **31** has a D-benzyl protected serine at **3** and valines substituted into positions **2**, **4**, and **5**. Both **30** and **31** were inactive relative to **23**. Analogously, compounds **32** and **33**, which contained a D-methylalanine at **3** were also both inactive. Interestingly, **23** with a D-valine at **3** is very potent with a nanomolar IC_{50} value, yet **34**, which contains valines substituted at **2**, **4**, and **5**, in addition to a D-valine at **3**, is not. Additional second generation compounds included substitutions at both the **3** and **4** positions or the **3** and **5** positions to explore if specific features that were critical to potency in the first generation could be utilized

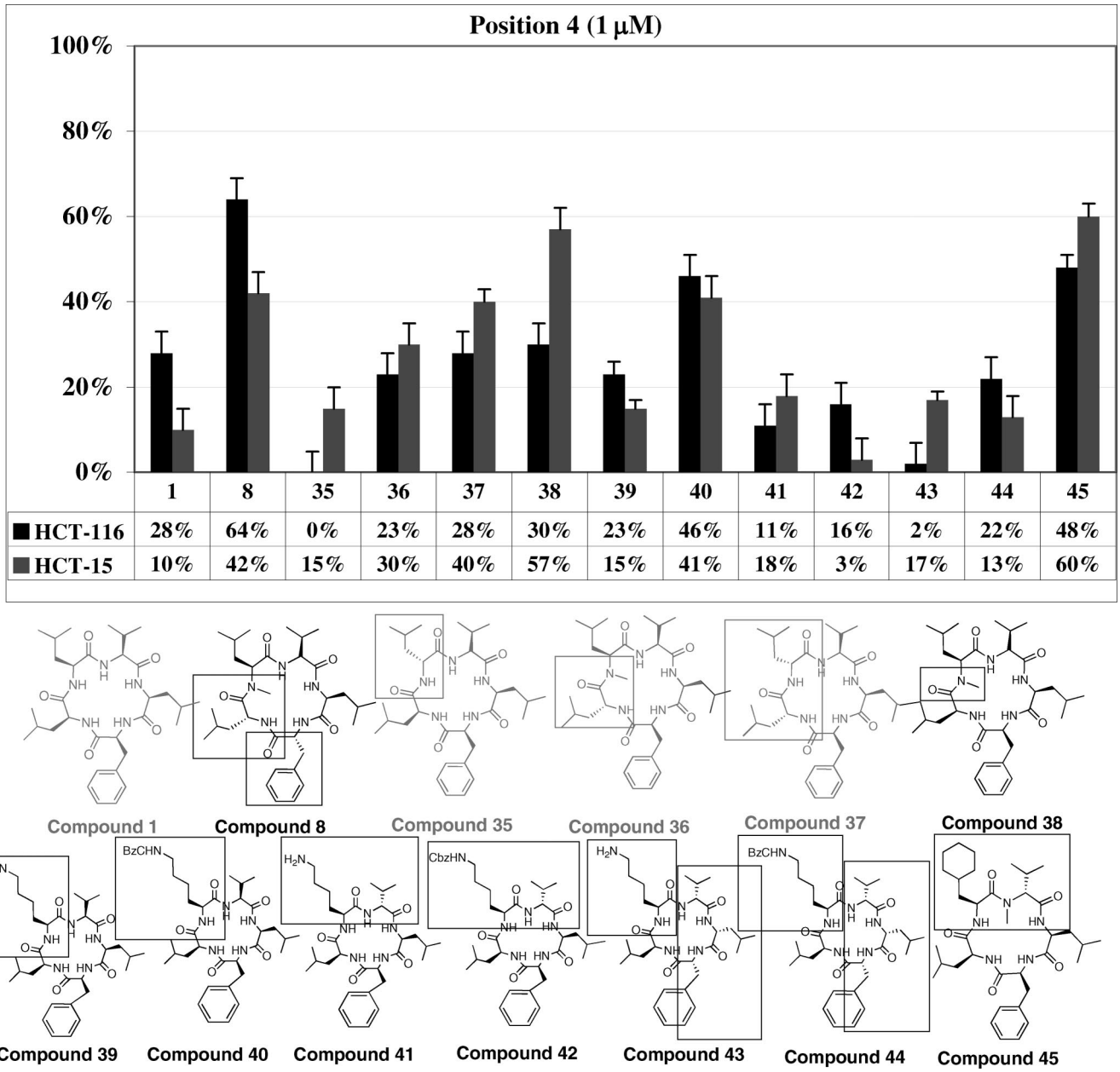

Figure 7. Compounds with changes to position **4**. Grey compounds **35**−**37** are first generation compounds, while black compounds **8**, **38**−**45** are second-generation.

synergistically to improve activity. These compounds will be discussed in Figures 7 and 8, respectively. Comparison of the IC_{50} values of first generation compound **23** and **1** (Figure 10), are 1.3 μM versus 25 μM in HCT-116 and 0.8 μM versus 46 μM in HCT-15, respectively. Thus, **23** is up to 60-fold more potent than **1**. Overall, one compound in the first-generation series, **23**, demonstrated a clear and significant improvement in growth inhibition maintaining greater than 45% against both cell lines.

Compounds **35**, **36**, and **37** are first generation compounds, (shown in gray, Figure 7), while compounds **8** and **38**−**45** are second-generation (shown in black). The first generation compounds involved incorporation of a D-aa at **4** (**35**), N-methyl at **4** and a D-aa at **5** (**36**), or two D-aas in positions **4** and **5** (**37**). None of these three compounds were active above 40% inhibition. For the second-generation compounds in Figure 7, we incorporated a number of aas that are different from those of the natural product primarily at position **4**. Potent compound **8** involved alterations at positions **1**, **4**, and **5** and its nanomolar/low micromolar IC_{50} values were discussed earlier. Compound **38** involved the incorporation of an N-methyl moiety at **4**, and although it showed some promise in HCT-15 cell lines (i.e., in the nanomolar potency), it did not show potential for growth inhibition against HCT-116. Compound **39** incorporates a lysine at position **4**, which greatly diminishes its potency relative to **1**. Interestingly, hydrophobic compound **40**, which contains a carboxybenzyl (Cbz)-protected lysine at **4**, is relatively active (averaging 43% against both cell lines). Yet, compound **41**, which incorporates a lysine at **4** and a D-valine at **3** and parallels **39** in structure is not potent, and neither is **42**, which contains a Cbz-protected lysine at **4** and a D-valine at **3**, paralleling **40**. It is interesting to note that both **41** and **42** contain the key element (a D-valine) that makes **23** so active, yet both of these compounds are not potent despite containing that residue at position **3**. Finally, neither polar compound **43** nor hydrophobically related derivative **44** are active (note: both contain three

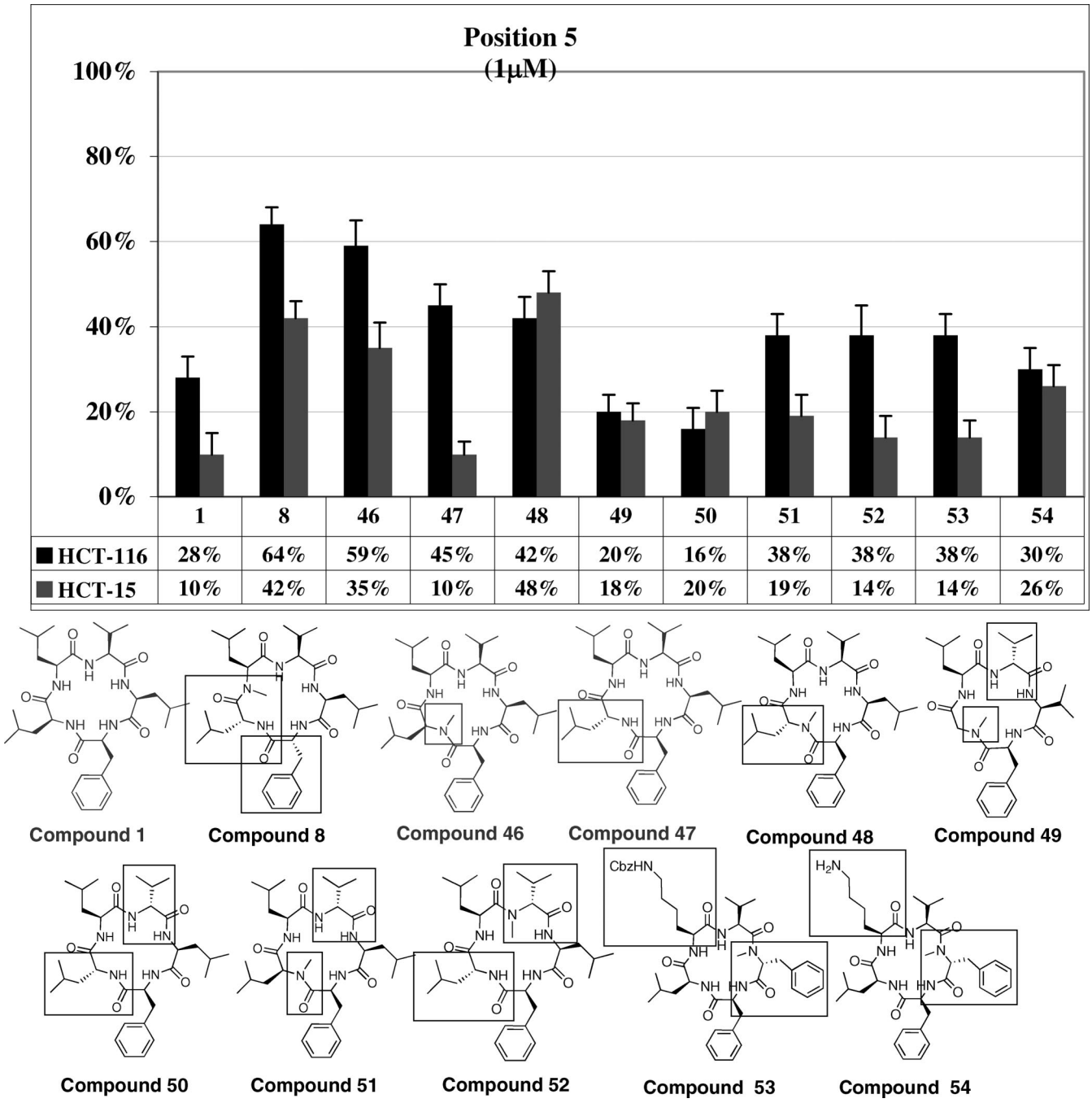

Figure 8. Compounds with changes to position **5**. Grey compounds **46** and **47** are first generation compounds, while black compounds **8**, **48**−**54** are second-generation.

D-aas at **1**, **2**, and **3**). Thus, polar moieties do not enhance the cytoxicity of compounds nor does the random incorporation of hydrophobicity (i.e., a Cbz-protected group). Rather, potency appears to be directly related to the specific conformation of the individual molecules. Finally, the incorporation of the potent element from position **3**, an N-methyl D-valine and a cyclohexyl moiety at **4**, generated compound **45**. This molecule is relatively potent, with IC_{50}s in the low micromolar and nanomolar range for the two cell lines. Thus, only two compounds, both second generation, had growth inhibition percentages greater than 45% in both cell lines: **8** and **45**. Both of these showed a significant increase in cytotoxicity over **1** and the first generation compounds. It is interesting to note that compound **40**, a second-generation compound, has a 43% average growth inhibition, yet structurally similar compounds **42** and **44** are inactive. This difference in potency is believed to be due to constraints imposed by the other residues within the macrocycle that lead to a specific conformation, ultimately allowing positive interactions and presentation of residues with its protein target for **40** or negative interactions in the case of **42** and **44**.

Compounds **46** and **47** are first generation compounds with substitutions focusing on position **5** (shown in gray, Figure 8), while compounds **8**, **48**−**54** are second-generation (shown in black). The first generation compounds involved incorporation of a D-aa at **5** (**47**), or an N-methyl (**46**). Both of these two compounds showed growth inhibition at ≥45% for HCT-116, but both showed low inhibition of HCT-15. For the second-generation compounds, potent compound **8** involved alterations at positions **1**, **4**, and **5** and its nanomolar/low micromolar IC_{50} values were discussed earlier. In addition, compound **48**

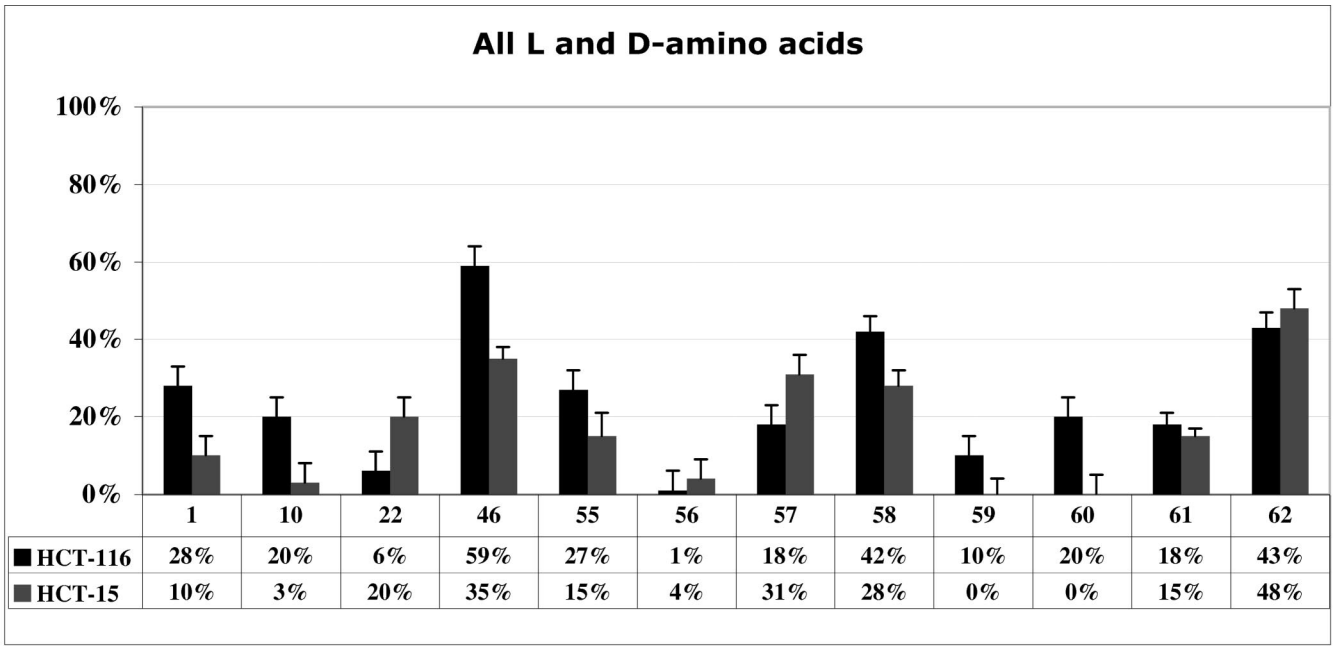

	1	10	22	46	55	56	57	58	59	60	61	62
HCT-116	28%	20%	6%	59%	27%	1%	18%	42%	10%	20%	18%	43%
HCT-15	10%	3%	20%	35%	15%	4%	31%	28%	0%	0%	15%	48%

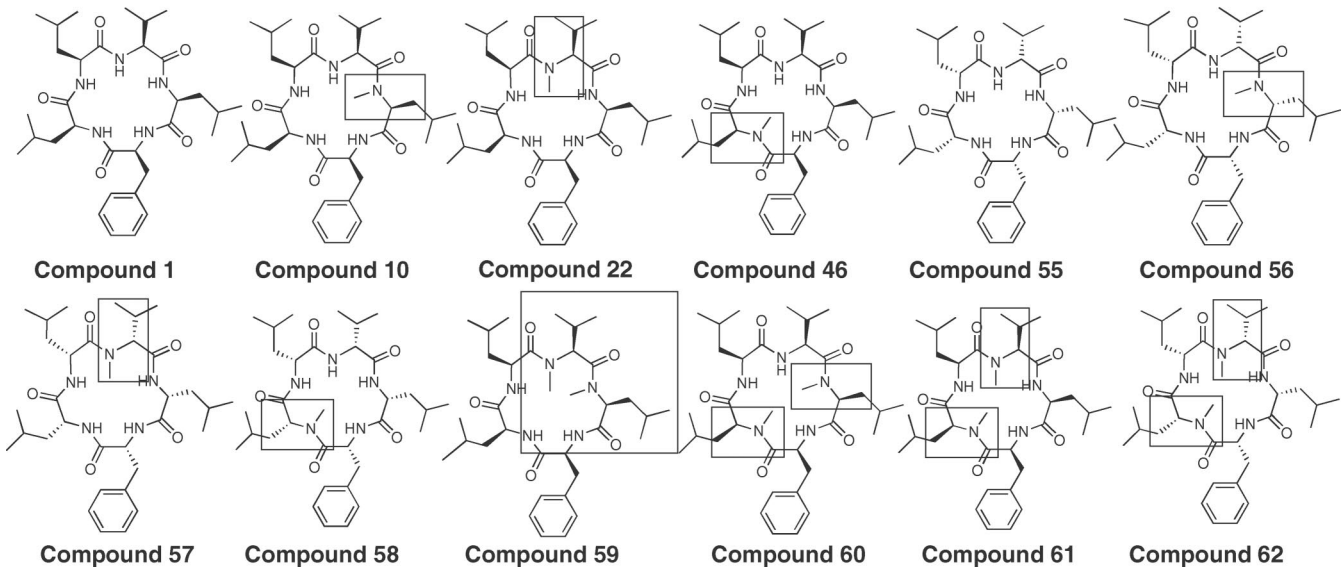

Figure 9. Compounds with N-methyl moieties and their enantiomers. All compounds are first generation.

involved the incorporation of an N-methyl D-aa at **5**, and it demonstrated reasonable potency with an average of potency of 45% for both cell lines (42% for HCT-116 and 48% for HCT-15). Thus, it is IC_{50} values were in the very low micromolar range (Figure 10). Compounds **49**, **50**, and **51**, which all contained the potent residue from **23** (a D-valine at position **3**), and substitutions at position **5** had reduced potency compared to the parent compounds **1**, **46**, **47**, or **23**. Thus, combined features do not generate synergistic cytotoxic effects. Compound **52**, which contained an active N-methyl residue at **3** and a D-leucine at **5** [based on **47**] showed no growth inhibition in either cell line. Finally, compounds **53** and **54**, which incorporated the potent residue from **14**, an N-methyl D-phenylalanine at **2**, and a Cbz-protected lysine or lysine at **4**, respectively, both exhibited lower activity than **14**. Thus, although two first generation compounds, **46** and **47**, both showed potency against HCT-116, only one compound (**8**), which is a second-generation molecule, had growth inhibition percentages greater than 45% in both cell lines.

Interestingly, comparing compounds with N-methyls at various positions to their enantiomers indicates that two compounds are relatively active (Figure 9). One is compound **46**; as discussed earlier, it contains an N-methyl at position **5**. In addition, compound **62**, which has all D-aas and an N-methyl on both positions **3** and **5**, appears to be relatively active. Intriguingly, compounds **58** and **61**, which are enantiomers of **46** and **62**, respectively, are not active, indicating their biological target is chiral.

The IC_{50} values for the most potent compounds are shown in Figure 10. Compound **14** has nanomolar IC_{50} values for both colon cancer lines, it is ~70-fold more active than the parent natural product peptide **1**, and it shows greater than 250-fold differential selectivity for colon cancer cells over normal cells (WS1 skin fiber blasts). Gemcitabine was used as a control compound, as it is currently used for treating a number of cancers, including pancreatic and colon cancers. Importantly, compound **14** shows ~15-fold greater potency than gemcitabine for inhibiting growth against these cancer cell lines. Thus, these

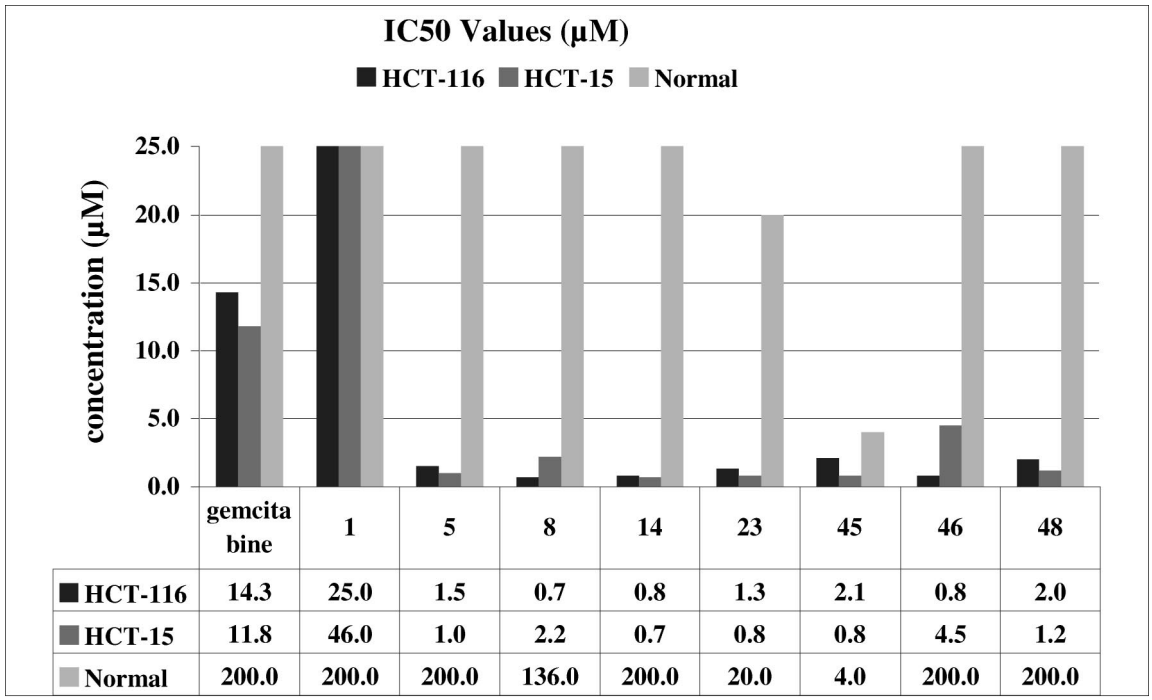

	gemcitabine	1	5	8	14	23	45	46	48
HCT-116	14.3	25.0	1.5	0.7	0.8	1.3	2.1	0.8	2.0
HCT-15	11.8	46.0	1.0	2.2	0.7	0.8	0.8	4.5	1.2
Normal	200.0	200.0	200.0	136.0	200.0	20.0	4.0	200.0	200.0

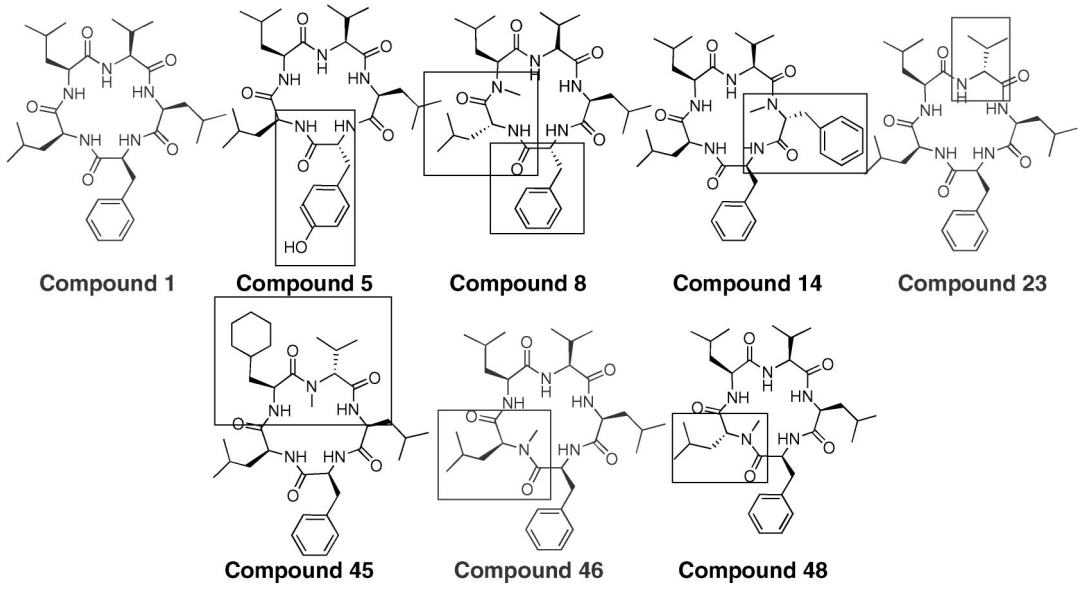

Figure 10. IC_{50} values of compounds run in three cell lines: HCT-116, HCT-15, and WS-1 (normal cells, skin fibroblasts). Data represents results from a concentration curve[29] taken from four concentrations, where each concentration data point is from three separate experiments performed in quadruplicate. Margin of error = ±5%; 200 μM is the outside limit of our detection.

San A-amide derivatives have greater potency than a current drug on the market, indicating their potential for use as a therapeutic agent.

Summary of SAR Results. After testing 62 compounds, we have come to the conclusion that no single feature or position is critical to potency but rather, as is typical in complex systems, there are several determining factors. The most important features to emerge from this SAR study involve the incorporation of a D-phenylalanine or D-tyrosine at position **1** (as observed for **8** and **5**, respectively), an N-methyl D-phenylalanine at **2** [seen in **14**], a D-valine at **3** [i.e., **23**], a hydrophobic moiety at **4** [as denoted by structures **45** and **40**], and finally an N-methyl L-leucine or an N-methyl D-leucine at **5**[contained in active compounds **8**, **46**, **47**, and **48**]. However, the combination of these structural elements does not provide synergistically active compounds. For example, compound **51**, which contains an N-methyl at **5** and a D-valine at **3**, demonstrates lower cytotoxicity than the "parent" compounds **23** or **46**. One very important aspect shown by this SAR is that polar compounds, regardless of the positional placement of the polar aa, are ineffective: **7**, **15**, **16**, **28**, **29**, **39**, **41**, **43**, and **54**. Yet, the additional substitution of relatively hydrophobic elements with correct placement are potent: compounds **14**, **40**, and **45**. Interestingly, compounds with elements that are more hydrophobic than the parent compound **1** and do not have the hydrophobic element correctly oriented, that is, **17**, **21**, **30**, **31**, **42**, **44**, and **53**, are not potent.

The key connection between potency and structure involves constraining the macrocycle into its active conformation and thus binding to its target in that position. Recent publications highlighted that a single N-methyl D-aa was the central structural component required to maintain a dominant

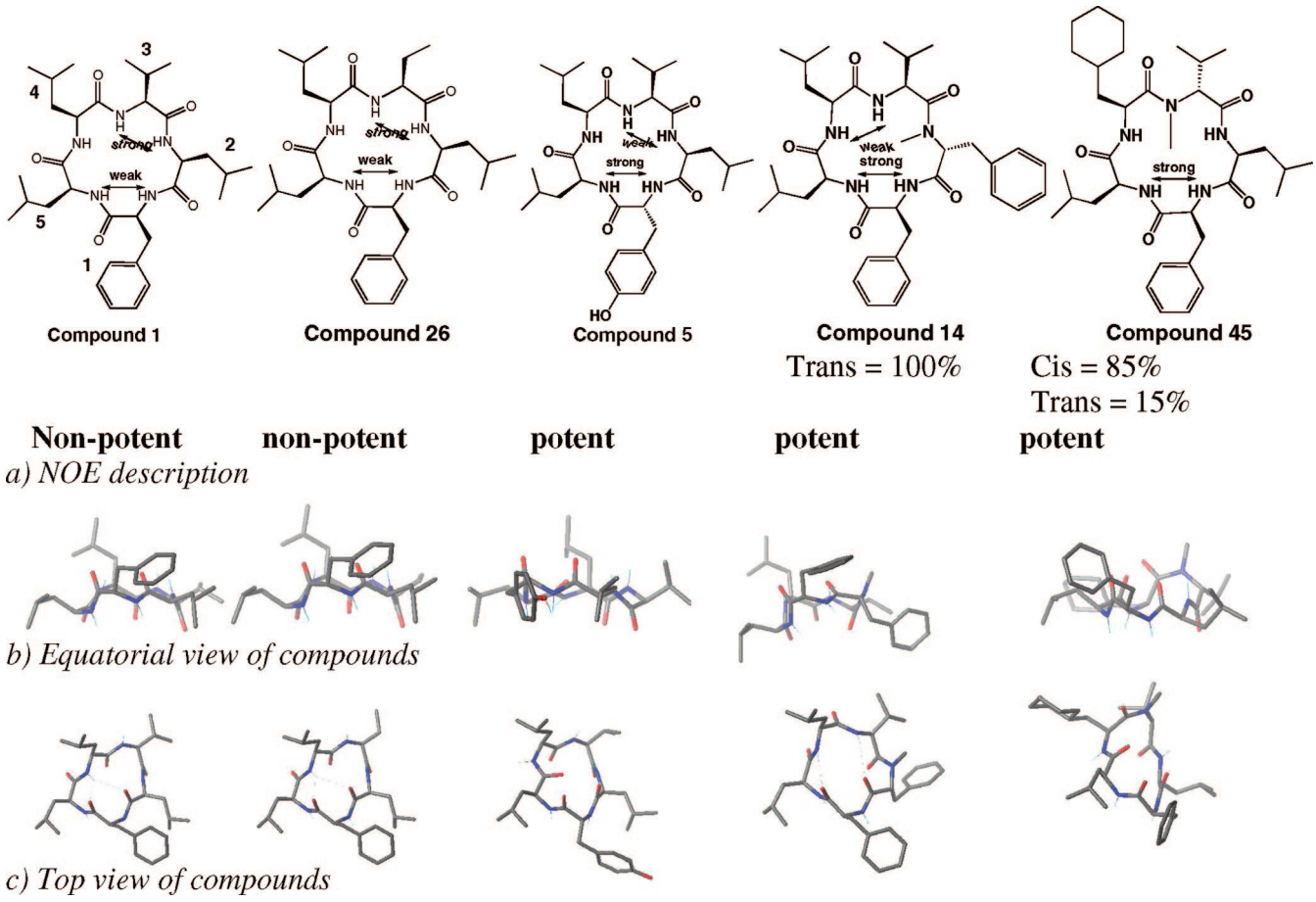

Figure 11. The NOEs (row a) and the 3D structures for five compounds, as determined by NMR (row b is equatorial view and row c is top view). Compounds **1** and **26** are inactive and **5**, **14**, and **45** are potent compounds.

conformation in macrocycles with five aas.[14,15,30] Thus, the inclusion of a *single* N-methyl D-aa in our active structures locks the ring into its low energy conformation, and this conformation appropriately presents the side chains to the biological target. Indeed, there is extensive evidence that cyclic peptides and, specifically, pentapeptides with a single D-aa lock the macrocycle into a single conformation.[14,15] Further, it is well established that these cyclic pentapeptides mimic beta and gamma turns and serve as templates for appropriately positioning suitable binding motifs for proteins.[16,17] Thus, out of the seven potent compounds described in Figure 10, six compounds follow this rule of a single N-methyl and D-aa: **5**, **14**, **23**, **45**, **46**, and **48**. Further, because all compounds are cyclic peptides, they have restricted bond rotations and are conformationally constrained, suggesting that their binding affinity for their target is greater than any small molecule.[20] In addition, all seven active compounds are lipophilic, thus, they are rapidly absorbed through membranes.[19] Indeed, any hydrophilic element that was substituted into the macrocycle greatly diminished their potency. Finally, these macrocycles are relatively straightforward to synthesize and can be made on multigram scale for further biological studies.

NMR Structural Studies. To explore the proposed hypothesis regarding a single N-methyl and D-aa locking the compound into an active position, we evaluated our compounds using NMR data and computational data. We determined the 3D structure of our compounds using TOCSY and NOESY experiments.[31] Note that the NOESY had stronger cross-peaks for these compounds than the ROESY. Spectra were acquired on a Bruker AV-800 instrument with a TCI cryoprobe operating at 800.23 MHz for ^{1}H. Samples were dissolved in DMSO-d_6 or 75% DMSO-d_6/25% H_2O at concentrations of 2–3 mg/mL. Shown in Figure 11 are the 3D structures and the NOEs observed between the amide protons of five compounds: **1**, **26**, **5**, **14**, and **45**. These five compounds were chosen because **1** represents the natural product peptide structure as a comparison molecule. Compound **26** is a nonactive compound and, therefore, represented a good negative control, whereas compounds **5**, **14**, and **45** are all active compounds and, therefore, could be used to determine a common structural motif.

Formally, a cyclic peptide must reverse the direction of the peptide chain twice relative to a linear peptide simply as a consequence of being cyclic. Four of the five compounds (**1**, **26**, **5**, and **14**) are observed to have two separated amide−amide NOEs. Compound **45** contains an N-methyl residue in the location where an amide−amide NOE might be expected. The NOE marker of a type II beta turn is a cross-peak between the amide protons of the third and fourth residue of the turn. However, this cross-peak appears for other turn types as well, and our previous experience has shown that small cyclic peptides may have turn types that deviate significantly from any of the standard turns.[32] The NMR data indicates that a structure has a turn-like structure centered on residues **1** and **2** correlates with the potency of the compound. Compounds **1** and **26** are the control structures as they are relatively nonpotent compared to **45**, **5**, and **14**. Both **1** and **26** show weak NOEs between positions **1** and **5**, whereas the potent compounds **45**, **5**, and **14** all show strong

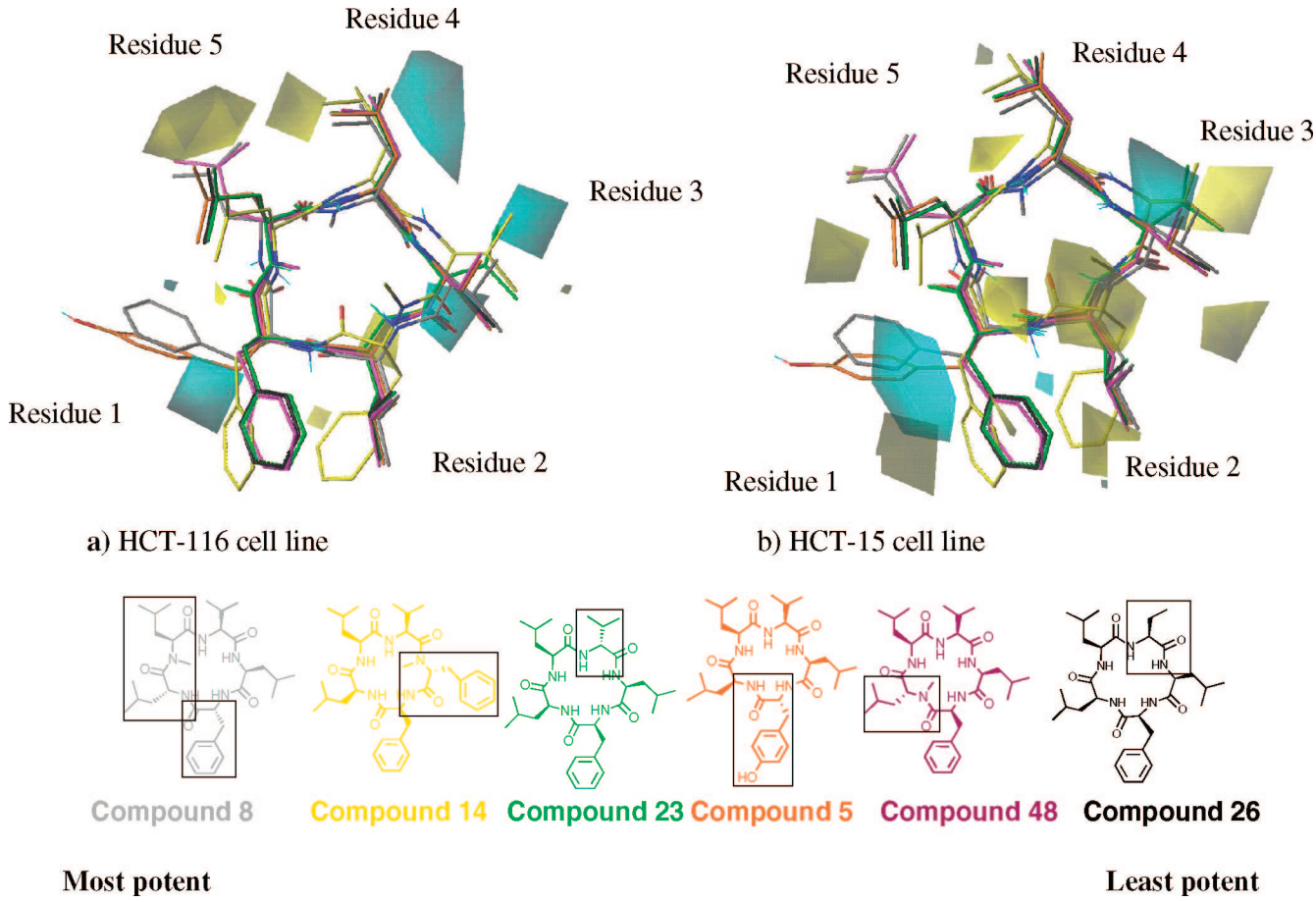

Figure 12. CoMFA steric features for the HCT116 (a) and HCT15 (b) in QSAR models are shown. Features correspond to isosurfaces of the product of the mean probe−ligand van der Waals interactions and the CoMFA coefficients, with yellow surfaces representing the most favorable 20% of the interaction space, and cyan surfaces representing the least favorable 20%. CoMFA pharmacophore map for the five most potent compounds (listed in order of most potent to least potent; **8**, **14**, **23**, **5**, and **48** in HCT-116 and in HCT-15 compared to nonpotent compound **26** are overlaid according to the following color scheme (listed most potent to least potent): **8** = gray, **14** = yellow, **23** = green, **5** = orange, **48** = magenta, and **26** = black. The cycle begins at the lower left, and residues 1−5 run counterclockwise around the cycle.

NOEs between **1** and **5**. In addition, compounds **1** and **26** show a strong NOE between positions **2** and **3**, yet, this is a weak NOE for **5**. Compound **14** also has a weak NOE but it is between **3** and **4** (because it has an N-methyl at **2**, it is unable to have an NOE between **2** and **3**).

From the 3D structures shown in Figure 11, it is apparent that nonpotent compounds **1** and **26** have very similar side chain positioning, whereas active compounds **5**, **14**, and **45** are structurally different from these control compounds. Although all three active compounds are not identical to each other in 3D structure, **5** and **14** have similar side chain orientations that can be seen via the top view (row c). Compound **45** has a distinctive 3D structure, presumably because of the high percentage of *cis*-amides present. This may also be responsible for the cytotoxicity of **45** against normal cell lines.

Molecular Modeling Studies Using CoMFA. All 62 compounds were analyzed by a CoMFA model[33] to understand their SAR and how it relates to structure. CoMFA modeling provides a projection of a pharmacophore map that is generated by fitting the experimental inhibition data to a partial least-squares fit (Figure 12). Although NMR data can be utilized using the CoMFA model, CoMFA is most frequently used to generate 3D structures using growth inhibition data. Our CoMFA structures were generated from the growth inhibition data on the HCT-116 and HCT-15 cancer cell lines, and we show that these structures generated using CoMFA are consistent with the 3D structures generated by NMR. The pharmacophore maps for each cell line were almost identical, indicating that the compounds were most likely reaching the same target in both cell lines. The aligned ligand manifolds were based on a conformer for the unmodified San A-amide pentapeptide (**1**). The conformer was derived from the linear chain analog of **1** (constructed in SYBYL[35] in a default β-sheet conformation using the biopolymer peptide builder) and using molecular dynamics simulation (Tripos force field).[36] The resulting structure was then optimized in SYBYL to within default molecular mechanics (MM) convergence criteria using the Tripos force field. This cyclization procedure was repeated five times using different molecular dynamic random seeds to ensure consensus in the predicted structure. Although these data are only a computational representative of the structural conformer, placing all five amide protons oriented above the pseudoplane of the ring systematically places all side chains in distinct regions of space, which generates a relatively reasonable model for qualitative SAR assessment. The full manifold of ligands were then constructed by initially conserving this backbone conformation, then allowing each San A-amide analog to relax via an unconstrained MM optimization (same force field and charges as above; default convergence settings). From the CoMFA analysis, it was observed that steric/van der Waals interactions accounted for 86% and 84% of the variable dependency for the HCT-116

and HCT-15 models, respectively. This agrees well with our qualitative assessment that polar residues afford no improvement in bioactivity relative to the hydrophobic aas.

For our QSAR analysis, we have thus focused variations in the steric profile of ligands, with the primary features, that is, pharmacophore maps for the HCT-116 and HCT-15 models being shown in Figure 12. Based on the above CoMFA analysis, we determined that the top scoring compounds are **8** and **14**, with compounds **23**, **5**, and **48** ranking close behind.[33] The CoMFA data strongly suggests that potency is enhanced when aas **1** and **5** have strong interactions (indicated by the yellow shape on the molecule). Importantly, strong interactions between residues **5** and **1** are also observed in the NOE data for the potent compounds **5**, **14**, and **45** (Figure 11),whereas the less potent compounds, **1** and **26**, both show weak NOEs between **1** and **5**. These strong interactions appear to be most enhanced when a D-aa is in positions **1** and **5** (**8**). Compound **5** may have scored well because of the hydrogen-bonding element on the D-tyrosine at **1**. A combination of a D-aa in **5** and a D-tyrosine at **1** is being synthesized. Positive interactions are also predicted when compounds contain a D-valine at position **3** and an L-aa at position **4** (the yellow shape indicates a positive interaction between the derivative and the protein target). These predictions are identical to those gathered from a visual inspection of our SAR data.

A number of interesting trends are evident in the CoMFA models. Placement of a D-phenylalanine at position **1** is generally unfavorable (indicated by cyan feature), except where the D-Phe at position **1** is capable of interacting with a D-leucine at position **5** (yellow feature). In HCT116, the L-Phe is also considered unfavorable (cyan feature on the bottom left) unless it interacts tangibly with another D-aa on position **2** (small yellow feature). A methylated amide at **2** (yellow feature) seems to be consistently favorable. Placement of an L-valine at position **3** is consistently considered unfavorable. Coupling between L-Leu side chains in positions **4** and **5** is a favorable feature for both cell lines. Collectively, this reveals complex interdependencies between the various diversity points in this scaffold. While this preliminary model provides useful insight in decoupling the various interdependencies, key enhancements are required to derive solid pharmacophore insight that extends beyond the confines of the San A-amide based scaffold. First of all, some ambiguities exist in the relative alignment of the various ligands in that compounds such as **14** and **13** have two phenylalanine residues, of which either one could plausibly align with the Phe-1 residue of San A-amide. Furthermore, a better understanding is required of the true bioactive conformer, in that the structural diversity inherent in the ligand manifold could dictate the presence of multiple distinct bioactive backbone conformers throughout the set of San A-amide analogs.

Conclusion

We report here for the first time a comprehensive evaluation of our two generations of compounds against several drug-resistant colon cancer cell lines. This global evaluation included the determination of specific features that generate active compounds in these two generations of derivatives, that is, placement of a single N-methyl and D-aa, which is responsible for the primary activity of these macrocyclic pentapeptides. In addition, it involves an extensive discussion on the 3D structures using NMR and CoMFA of the active compounds compared to inactive derivatives. Our most potent seven small molecules target these drug-resistant colon cancer cell lines at potencies that are significantly greater than those previously reported, share no homology with other classes of chemotherapeutic agents, and have reasonable ClogP values and molecular weights (450–600). Out of the seven most potent compounds reported here, five are second-generation compounds, emphasizing our ability to incorporate potent features found in the first-generation into the development of effective second-generation molecules. Thus, this class of compounds provides potential structures for further chemotherapeutic development. Importantly, the most potent compounds show 70-fold improved potency over the natural product peptide, 250-fold differential selectivity for colon cancer cells over normal cells, and 15-fold greater potency than a current drug on the market used to treat cancers. Assays determining the active compounds' mechanism of action are ongoing and will be reported in the near future.

Experimental Section

Thymidine Incorporation/Growth Inhibition Assay. Proliferation of the HCT-116, HCT-15 colon cancer, and WS-1 normal cell lines were tested in the presence and absence of the compounds using ^{3}H-thymidine uptake assays. Cells treated with the compounds were compared to DMSO-treated controls for their ability to proliferate as indicated by the incorporation of ^{3}H-thymidine into their DNA. Cells were cultured in 96-well plates at a concentration of 3000 cells/well. The media was IMDM for HCT-116, RPMI 1640 for HCT-15, and MEM for WS-1 with L-glutamine, 10% fetal bovine serum, and 0.1% penicillin-streptomycin antibiotics. After incubation for approximately 6 h, the compounds were added. The compounds were dissolved in DMSO at a final concentration of 2 mM and tested at the concentrations indicated in the manuscript. The DMSO concentration was held constant in all wells at 1%. After the cells had been incubated with the compounds for 56 h, 1 mCi ^{3}H-thymidine per well was added and the cells were cultured for an additional 16 h (for the cells to have a total of 72 h with the drug), at which time the cells were harvested using a PHD cell harvester from Cambridge Technology Incorporated. The samples were then counted in a scintillation counter for 2 min each using ScintiVerse universal scintillation fluid from Fisher. Decreases in ^{3}H-thymidine incorporation, as compared to controls, are an indication that the cells are no longer progressing through the cell cycle or synthesizing DNA, as is shown in the studies presented.

Synthesis. For synthesis details of the first-generation compounds, see ref 4. For second-generation compounds, see ref 5. The final characterization data of the potent compound are listed below.

NMR Structural Experiments. Spectra were acquired on a Bruker AV-800 instrument with a TCI cryoprobe operating at 800.23 MHz for ^{1}H. Samples were dissolved in DMSO-d_6 or 75% DMSO-d_6/25% H_2O at concentrations of 2–3 mg/mL. The 2D experiments were done with the standard Bruker parameters and pulse programs dipsi2esgpph and noesyesgpph, with water suppression provided by excitation sculpting.

Molecular Modeling Studies Using CoMFA. In these preliminary models, the aligned ligand manifolds were based on a conformer for the unmodified San A-amide pentapeptide (**1**). The conformer was derived from the linear chain analog of **1** (constructed in SYBYL[34] in a default β-sheet conformation using the biopolymer peptide builder) and using molecular dynamics simulation (Tripos force field).[35] The resulting structure was then optimized in SYBYL to within default MM convergence criteria using the Tripos force field. This cyclization procedure was repeated five times using different molecular dynamic random seeds to ensure consensus in the predicted structure. Although these data are only a computational representative of the structural conformer, placing all five amide protons oriented above the pseudoplane of the ring

systematically places all side chains in distinct regions of space, which generates a relatively reasonable model for qualitative SAR assessment. The full manifold of ligands were then constructed by initially conserving this backbone conformation, then allowing each San A-amide analog to relax via an unconstrained MM optimization (same force field and charges as above; default convergence settings).

For the HCT116 assay (57 molecules in the original set), a strongly correlating ($R^2 = 0.92$; $Q^2_{LOO} = 0.74$) four-component model was obtained after discarding four inactive members of the training set (compounds **13**, **25**, **28**, and **52**, respectively). The 5-fold (FF) cross-validation experiments attest to exceptional stability and predictivity in the model, with $Q^2_{FF} = 0.72$. For HCT15 (55 molecules), a solid five-component representation ($R^2 = 0.95$; $Q^2_{LOO} = 0.71$) was attained after discarding five inactive ligands (compounds **5**, **13**, **15**, **9**, and **52**). The model also exhibits good stability and internal predictivity ($Q^2_{FF} = 0.64$). From the CoMFA analysis, it was observed that steric/van der Waals interactions accounted for 86 and 84% of the variable dependency for the HCT116 and HCT15 models, respectively. This agrees well with our qualitative assessment that polar residues afford no improvement in bioactivity relative to the hydrophobic Phe, Leu, and Val aas. We trained our CoMFA models to the natural logarithmic quantity log[inh. %]. In an attempt to capture tangible information from inactive compounds, we circumvented the undefined nature of log[0] by arbitrarily specifying small nonzero inhibition values of 0.001% (i.e., log[inh. %] = −6.91) for inactive species. CoMFA interaction terms for the ligand manifold were computed using the Tripos Standard Field probe, including both steric and electrostatic field components, with the latter incorporating a distance-based dielectric modulation. Field cut-offs and smoothing protocols were set according to default values. CoMFA model training and evaluation were then utilized via the SAMPLS algorithm,[36] which reports leave-one-out cross-validated Q^2_{LOO} values for the PLS-fitted model. To ensure a robust, correlative, predictive, and statistically significant model, we iteratively discarded the maximally outlying molecule in each training set until a core manifold was obtained whose Q^2_{LOO} value was greater than 0.60 for a number of PLS components not exceeding $^1/_7$th of the total number of molecules under consideration.

Acknowledgment. We thank San Diego State University for financial support.

Supporting Information Available: A table that includes the description of all changes made to compound structures in text format and IC_{50} data curves are supplied. This material is available free of charge via the Internet at http://pubs.acs.org.

References

(1) Cueto, M.; Jensen, P. R.; Fenical, W. N-Methylsansalvamide, a cytotoxic cyclic depsipeptide from a marine fungus of the genus *Fusarium*. *Phytochemistry* **2000**, *55*, 223–226.

(2) Hwang, Y.; Rowley, D.; Rhodes, D.; Gertsch, J.; Fenical, W.; Bushman, F. Mechanism of inhibition of a poxvirus topoisomerase by the marine natural product Sansalvamide A. *Mol. Pharmacol.* **1999**, *55*, 1049–1053.

(3) Belofsky, G. N.; Jensen, P. R.; Fenical, W. Sansalvamide: A new cytotoxic cyclic depsipeptide produced by a marine fungus of the genus *Fusarium*. *Tetrahedron Lett.* **1999**, *40*, 2913–2916.

(4) Styers, T. J.; Kekec, A.; Rodriguez, R.; Brown, J. D.; Cajica, J.; Pan, P.-S.; Parry, E.; Carroll, C. L.; Medina, I.; Corral, R.; Lapera, S.; Otrubova, K.; Pan, C.-M.; McGuire, K. L.; McAlpine, S. R. Synthesis of Sansalvamide A derivatives and their cytotoxicity in the colon cancer cell line HT-29. *Bioorg. Med. Chem.* **2006**, *14*, 5625–5631.

(5) Rodriguez, R.; Pan, P.-S.; Pan, C.-M.; Ravula, S.; Lapera, S.; Singh, E.; Styers, T. J.; Brown, J. D.; Cajica, J.; Parry, E.; Otrubova, K.; McAlpine, S. R. Synthesis of second generation Sansalvamide A derivatives: Novel templates as potent antitumor agents. *J. Org. Chem.* **2007**, *72*, 1980–2002.

(6) Liu, S.; Gu, W.; D, L.; Ding, X.-Z.; Ujiki, M.; Adrian, T. E.; Soff, G. A.; Silverman, R. B. N-Methylsansalvamide A peptide analogues. Potent new antitumor agents. *J. Med. Chem.* **2005**, *48*, 3630–3638.

(7) Pan, P.-S.; McGuire, K. L.; McAlpine, S. R. Identification of compounds potent against pancreatic cancer cell lines. *Bioorganic and Med. Chem. Lett.* **2007**, *17*, 5072–5077.

(8) Ujiki, M.; Milam, B.; Ding, X.-Z.; Roginsky, A. B.; Salabat, M. R.; Talamonti, M. S.; Bell, R. H.; Gu, W.; Silverman, R. B.; Adrian, T. E. A novel peptide sansalvamide A analogue inhibits pancreatic cancer cell growth through G0/G1 cell-cycle arrest. *Biochem. Biophys. Res. Commun.* **2006**, *340*, 1224–1228.

(9) Otrubova, K.; Styers, T. J.; Pan, P.-S.; Rodriguez, R.; McGuire, K. L.; McAlpine, S. R. Synthesis and novel structure−activity relationships of potent Sansalvamide A derivatives *Chem. Commun.* **2006**, 1033–1034.

(10) Carroll, C. L.; Johnston, J. V. C.; Kekec, A.; Brown, J. D.; Parry, E.; Cajica, J.; Medina, I.; Cook, K. M.; Corral, R.; Pan, P.-S.; McAlpine, S. R. Synthesis and cytotoxicity of novel Sansalvamide A derivatives. *Org. Lett.* **2005**, *7*, 3481–3484.

(11) Lee, Y.; Silverman, R. B. Rapid, high-yield, solid-phase synthesis of the antitumor antibiotic Sansalvamide A using a side-chain-tethered phenylalanine building block. *Org. Lett.* **2000**, *2*, 3743–3746.

(12) Gu, W.; Liu, S.; Silverman, R. B. Solid-phase, Pd-catalyzed silicon-aryl carbon bond formation. Synthesis of Sansalvamide A peptide. *Org. Lett.* **2002**, *4*, 4171–4174.

(13) A total of 80–85% of colon cancers are considered treatable using current chemotherapeutic drugs. The remaining 15–20% of colon cancers are drug-resistant colon cancers. The two types of colon cancers are referred to as MSS for the drug-sensitive colon cancers and MSI for the drug-resistant colon cancers. MSS (drug-sensitive) have an $IC_{50} \sim 5\ \mu M$.

(14) Chatterjee, J.; Mierke, D. F.; Kessler, H. N-methylated cyclic pentaalanine peptides as template structures. *J. Am. Chem. Soc.* **2006**, *128*, 15164–15172.

(15) Heller, M.; Sukopp, M.; Tsomaia, N.; John, M.; Mierke, D. F.; Reif, B.; Kessler, H. The conformation of cyclo(-D-pro-ala-) as a model for cyclic pentapeptides of the DL type. *J. Am. Chem. Soc.* **2006**, *128*, 13806–13814.

(16) Tyndall, J. D.; Pfieiffer, B.; Abbenante, G.; Fairlie, D. P. Over one hundred peptide-activated G protein-coupled receptros recognized ligands with turn structure. *Chem. Rev.* **2005**, *105*, 793–826.

(17) Viles, J. H.; Mitchell, J. B.; L., G. S.; Doyle, P. M.; harris, C. J.; Sadler, P. J.; Thornton, J. M. Multiple solution conformations of the integrin-binding cyclic pentapeptide cyclo(Ser-D-Leu-Asp-Val-Pro) analysis of the (phi, psi) space available to the cyclic pentapeptides. *Eur. J. Biochem.* **1996**, *242*, 352–362.

(18) The ClogP values were calculated using an algorithm. The logP value of a compound, which is the logarithm of its partition coefficient between *n*-octanol and water $\log(c_{octanol}/c_{water})$, is a well established measure of the compound's hydrophilicity. Low hydrophilicities and, therefore, high logP values cause poor absorption or permeation. It has been shown for compounds to have a reasonable probability of being well absorbed, their logP value must not be greater than 5.0. The distribution of calculated logP values of more than 3000 drugs on the market underlines this fact.

(19) Amidon, G. L.; Lee, H. J. Absorption of peptide and peptidimimetic drugs. *Annu. Rev. Pharmacol. Toxicol.* **1994**, *34*, 321–341.

(20) Wenger, R. M. Synthesis of cyclosporin and analogues: Structural and conformational requirements for immunosuppressive activity. *Prog. Allergy* **1986**, *38*, 46–64.

(21) Marx, V. Watching peptide drugs grow up. *Chem. Eng. News* **2005**, *83*, 17–24.

(22) Marx, V. Giving biotechnology a chemical push. *Chem. Eng. News* **2005**, *83*, 17–24.

(23) Loffet, A. Peptides as drugs: Is there a market. *Eur. Pept. Soc.* **2002**, *8*, 1–7.

(24) Styers, T. J.; Rodriguez, R.; Pan, P.-S.; McAlpine, S. R. High-yielding macrocyclization conditions used in the synthesis of novel Sansalvamide A derivatives. *Tetrahedron Lett.* **2006**, *47*, 515–517.

(25) Dipeptide and tripeptide structures were confirmed using ^{1}H NMR. All linear pentapeptides were confirmed using LCMS and ^{1}H NMR.

(26) Unpublished results from the Guy lab at the Department of Chemical Biology and Therapeutics, St Jude Children's Research Hospital, Memphis, TN 38103, and published results from our lab show that the use of several coupling reagents facilitates formation of the peptide bond in high yields.

(27) Bolla, M. L.; Azevedo, E. V.; Smith, J. M.; Taylor, R. E.; Ranjit, D. K.; Segall, A. M.; McAlpine, S. R. Novel antibiotics: Macrocyclic peptides designed to trap Holliday junctions. *Org. Lett.* **2003**, *5*, 109–112.

(28) Liotta, L. A.; Medina, I.; Robinson, J. L.; Carroll, C. L.; Pan, P.-S.; Corral, R.; Johnston, J. V. C.; Cook, K. M.; Curtis, F. A.; Sharples, G. J.; McAlpine, S. R. Novel antibiotics: Second generation macro-

cyclic peptides designed to trap Holliday junctions. *Tetrahedron Lett.* **2004**, *45*, 8447–8450.
(29) Concentration curves used to generate the IC_{50} data are shown in the Supporting Information.
(30) Zhang, X.; Nikiforovich, G. V.; Marshall, G. R. Conformational templates for rational drug design: Flexibility of cyclo(D-Pro[1]-Ala[2]-Ala[3]-Ala[4]-Ala[5]) in DMSO solution. *J. Med. Chem.* **2007**, *50*, 2921−2925.
(31) NOESY data showed stronger cross peaks than ROESY data.
(32) Liederer, B. M.; Fuchs, T.; Vander Velde, D.; Siahaan, T. J.; Borchardt, R. T. Effects of amino acid chirality and the chemical linker on the cell permeation characteristics of cyclic prodrugs of opioid peptides. *J. Med. Chem.* **2006**, *49*, 1261–1270.
(33) CoMFA determines the most likely conformation of the active compounds and establishes specific interactions that appear important for cytotoxicity. CoMFA is a modeling projection of a pharmacophore map, as derived by partial least squares, which are fit to experimental inhibition data by a weighted sum of spatial interaction terms between a probe atom and a manifold of related ligand structures. These interaction terms are carefully aligned according to conserved structural features.
(34) *SYBYL 7.2*, The Tripos Associates, St. Louis, MO 20006.
(35) Clark, M.; Cramer, R. D. I.; Van Opdenbosch, N. Validation of the general purpose Tripos 5.2 force field. *J. Comput. Chem.* **1989**, *10*, 982–1012.
(36) Bush, B. L.; Nachbar, R. B. Sample-distance partial least squares: PLS optimized for many variables, with application to CoMFA. *J. Comput.-Aided Mol. Des.* **1993**, *7*, 587–619.

JM070731A